TECHNICAL REPORT RD–AS–95–2

HIGH–FREQUENCY RADAR TARGET MODELING

Virginia C. Monk
Fred W. Sedenquist
Advanced Sensors Directorate
Research, Development, and Engineering Center

January 1995

U.S. ARMY MISSILE COMMAND
Redstone Arsenal, Alabama 35898–5000

Approved for public release; distribution is unlimited.

DESTRUCTION NOTICE

FOR CLASSIFIED DOCUMENTS, FOLLOW THE PROCEDURES IN DoD 5200.22-M, INDUSTRIAL SECURITY MANUAL, SECTION II-19 OR DoD 5200.1-R, INFORMATION SECURITY PROGRAM REGULATION, CHAPTER IX. FOR UNCLASSIFIED, LIMITED DOCUMENTS, DESTROY BY ANY METHOD THAT WILL PREVENT DISCLOSURE OF CONTENTS OR RECONSTRUCTION OF THE DOCUMENT.

DISCLAIMER

THE FINDINGS IN THIS REPORT ARE NOT TO BE CONSTRUED AS AN OFFICIAL DEPARTMENT OF THE ARMY POSITION UNLESS SO DESIGNATED BY OTHER AUTHORIZED DOCUMENTS.

TRADE NAMES

USE OF TRADE NAMES OR MANUFACTURERS IN THIS REPORT DOES NOT CONSTITUTE AN OFFICIAL ENDORSEMENT OR APPROVAL OF THE USE OF SUCH COMMERCIAL HARDWARE OR SOFTWARE.

UNCLASSIFIED

SECURITY CLASSIFICATION OF THIS PAGE

REPORT DOCUMENTATION PAGE

Form Approved
OMB No. 0704-0188
Exp. Date: Jun 30, 1986

1a. REPORT SECURITY CLASSIFICATION UNCLASSIFIED	1b. RESTRICTIVE MARKINGS
2a. SECURITY CLASSIFICATION AUTHORITY	3. DISTRIBUTION / AVAILABILITY OF REPORT Approved for public release; distribution is unlimited.
2b. DECLASSIFICATION / DOWNGRADING SCHEDULE	
4. PERFORMING ORGANIZATION REPORT NUMBER(S) TR–RD–AS–95–2	5. MONITORING ORGANIZATION REPORT NUMBER(S)
6a. NAME OF PERFORMING ORGANIZATION Advanced Sensors Directorate RD&E Center 6b. OFFICE SYMBOL (If applicable) AMSMI–RD–AS–MM	7a. NAME OF MONITORING ORGANIZATION
6c. ADDRESS (City, State, and ZIP Code) Commander, U. S. Army Missile Command ATTN: AMSMI–RD–AS–MM Redstone Arsenal, AL 35898–5253	7b. ADDRESS (City, State, and ZIP Code)
8a. NAME OF FUNDING / SPONSORING ORGANIZATION 8b. OFFICE SYMBOL (If applicable)	9. PROCUREMENT INSTRUMENT IDENTIFICATION NUMBER
8c. ADDRESS (City, State, and ZIP Code)	10. SOURCE OF FUNDING NUMBERS PROGRAM ELEMENT NO. / PROJECT NO. / TASK NO. / WORK UNIT ACCESSION NO.

11. TITLE (Include Security Classification)
High–Frequency Radar Target Modeling

12. PERSONAL AUTHOR(S)
Virginia C. Monk and Fred W. Sedenquist

13a. TYPE OF REPORT	13b. TIME COVERED	14. DATE OF REPORT (Year, Month, Day)	15. PAGE COUNT
Summary	FROM _____ TO Sep 94	January 1995	32

16. SUPPLEMENTARY NOTATION

17. COSATI CODES			18. SUBJECT TERMS (Continue on reverse if necessary and identify by block number)
FIELD	GROUP	SUB-GROUP	Radar Cross Section (RCS), Geometrical Optics (GO), Geometrical Theory of Diffraction (GTD), Uniform Theory of Diffraction (UTD), Method of Equivalent Currents (MEC), (Continued on Page ii)

19. ABSTRACT (Continue on reverse if necessary and identify by block number)

This report contains the theories behind the commonly accepted electromagnetic techiques used for Radar Cross Section (RCS) prediction and enumerates the prevailing computer models which characterize RCS for high–frequency complex targets.

20. DISTRIBUTION / AVAILABILITY OF ABSTRACT ☐ UNCLASSIFIED/UNLIMITED ☒ SAME AS RPT. ☐ DTIC USERS	21. ABSTRACT SECURITY CLASSIFICATION UNCLASSIFIED
22a. NAME OF RESPONSIBLE INDIVIDUAL Virginia C. Monk	22b. TELEPHONE (Include Area Code) (205) 876–2946 22c. OFFICE SYMBOL AMSMI–RD–AS–MM

DD FORM 1473, 84 MAR

83 APR edition may be used until exhausted.
All other editions are obsolete.

SECURITY CLASSIFICATION OF THIS PAGE
UNCLASSIFIED

18. SUBJECT TERMS (Continued)

Physical Optics (PO), Physical Theory of Diffraction (PTD), XPATCH, Radar Cross Section – Basic Scattering Code (RCS–BSC), Simulated Radar Image (SRIM), MAX–TRACK

TABLE OF CONTENTS

LIST OF ILLUSTRATIONS

I. INTRODUCTION

For years radar developers have been trying to evolve computer based models to accurately represent expected radar targets. Traditionally, targets have had their radar "signature" measured by actually recording the returned signals from the target of interest and building a database for characterization and analysis. This is an expensive process. Each individual target must be physically present to have its signature characterized.

Deriving a radar signature model through the use of a three–dimensional target–drawing database (not requiring the physical target present) has long been the dream of radar developers. This model would provide a cost effective alternative to real data collections and would allow exploiting the full capability of the radar's operational parameters. Through today's computational ability, the dream of an automated and systematic approach to theoretical Radar Cross Section (RCS) prediction is possible.

This paper will present the theories behind the commonly accepted electromagnetic techniques used for RCS prediction and enumerate the prevailing computer models which characterize RCS for high–frequency complex targets.

II. RADAR CROSS SECTION PREDICTION

The RCS of a target is a measure of power reflected back toward the radar when illuminated by an incident wave. RCS gives the target characteristics without including the effects of transmitter power, receiver sensitivity, or distance. IEEE defines RCS as a measure of reflective strength of a target defined as 4π times the ratio of the power per unit solid angle scattered in a specified direction to the power per unit area in a plane wave incident on the scatterer from a specified direction [12]. The formal definition is

$$\sigma = \lim_{R \to \infty} 4\pi R^2 \frac{|E_s|^2}{|E_o|^2}$$

where R is the distance between the radar and target, E_s is the field strength at the radar receiver due to the target reflection or scattering, and E_o is the incident field strength at the target [11]. The requirement for infinite range is made so that far field (plane wave) scattering can be assured. The problem of predicting RCS becomes one of determining the scattered field for plane–wave illumination.

The scattering wave breaks into three regions: (1) the low–frequency or Rayleigh region where the wavelength is much longer than the scattering body size and the scattering process is due to induced dipole moments where only gross size and shape of the body are of importance; (2) the resonant region, where the wavelength is on the same order as the body size and the scattering process is due to surface waves and optics; and (3) the high–frequency region where the wavelength is much smaller than the body and the scattering process is principally a summation of the returns from isolated, noninteracting scattering centers [12]. These regions do not refer to the actual frequency of the incident wave but to the size of the target when compared to the incident wavelength.

The calculation of the RCS for a complex target involves: (1) target modeling where the geometry of the target's exterior surfaces, ducts, wedges, apertures, and discontinuities must be described in terms of mathematical models; and (2) the computation of scattered electromagnetic fields which arise from different mechanisms such as specular reflection, diffraction, and multiple scattering [27]. To model the above, these scattering mechanisms and their sources must be known.

III. RADAR CROSS SECTION PREDICTION TECHNIQUES

The basic procedure for predicting the RCS of a target is to subdivide the target into a collection of simple elements such as flat plates, cylinders, and spheriods and assume that each scatterer is independent of all the other scatterers. There are a number of well established theoretical techniques for predicting the local scattering of electromagnetic radiation for high–frequency RCS prediction. These techniques include Geometrical Optics (GO), the Geometrical Theory of Diffraction (GTD), developments from GTD such as the Uniform Theory of Diffraction (UTD), Method of Equivalent Currents (MEC), Physical Optics (PO), and the Physical Theory of Diffraction (PTD) [15].

These techniques must interact with one another to be able to predict a complete RCS. For example, GO fails when one or both radii of curvature become infinite, such as in a cylinder or flat plate, so we would have to use PO to obtain this information. The techniques cited above are addressed in this section.

A. Geometrical Optics

The GO method is a high–frequency approximation where the scattering mechanism and energy propagation are accounted for by classical tubes of rays [4]. It is best used for ray tracing that does not encounter shadow boundaries and caustics. Implementation of GO requires that there exist a specular point on the body and that the principal radii of curvature be stipulated. The principle components of GO include: ray paths, ray spreading, and reflection coefficients [10].

GO is a ray–tracing procedure where the wavelength is allowed to become infinitesimally small. The energy propagates along slender tubes (rays) according to

$$u = Pe^{ikS}$$

where u represents the complex amplitude of a magnetic or electric field component transverse to the direction of propagation. Magnitude P and the phase factor S are functions of position in space and may be complex numbers. Propagation is in the direction given by ΔS. Surfaces of constant S are surfaces of constant phase. This equation is not valid near discontinuities such as edges [11].

When an incident ray strikes a smooth flat surface separating two media, part of the energy is reflected and part is transmitted across to the second medium. Snell's law indicates that the transmitted ray propagates in a direction different from that of the incident ray (refraction), and the angle of the reflected ray, as measured from the surface normal, is equal to the angle of the incident ray [11]. The amplitude and phase of the reflected ray are given by Fresnel reflection coefficients [10].

The decay or increase in energy can be calculated. If all the energy which entered the tube at one end is transmitted to the other, the ratio of power density at the output to that at the input is

$$\frac{|E_s|^2}{|E_o|^2} = \frac{\rho_1 \rho_2}{(s + \rho_1)(s + \rho_2)}$$

where E(s) is the field intensity at the output, E(o) is the field intensity at the input, s is the distance between the ends of the ray tube, and ρ_1 and ρ_2 are the principal radii of the curvature of the output wavefront [11]. The curvature relationship may be placed in the ratio of power density at the output to that at the input and then into the RCS formal definition, where s becomes R. If R is forced to infinity, the angular dependence on the local angle of arrival of the incident ray disappears; also, the angular rotation of the principal planes of the body radii of curvature also disappears. The result is

$$\sigma = \pi a_1 a_2$$

where a_1 and a_2 are the principal radii of the body at the specular point. One of the problems in computational schemes is the identification of the specular point.

This simple equation may be used for bistatic as well as monostatic cases as long as there is no forward direction. It may be used for metallic bodies, but the specular reflection must be multiplied by the reflection coefficient if the body is dielectric. Dielectric bodies are characterized by rays that penetrate the body as well as those reflected by the surface [11].

In GO approximation, the region of space is divided into distinct illuminated and shadow regions; therefore, this method cannot account for any diffraction effect [4]. Also, GO cannot take care of the phase of the field, caustic regions, shadow boundaries, or shadow region fields [4].

B. Geometrical Theory of Diffraction

J. B. Keller extended GO in GTD to include regions where diffracted fields are important, such as in shadowing [4]. GTD contains diffracted ray paths, including surface rays, and diffraction coefficients [10]. Figure 1 displays examples of diffracted rays for edge, wedge, corner tip, multiple diffracted, and curvature [10].

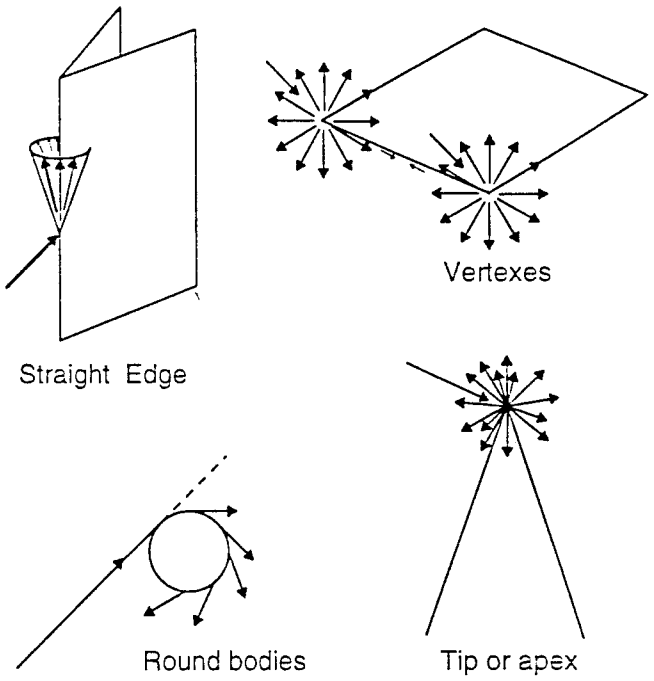

Figure 1. Diffraction Mechanisms

Reference 10 shows that the general form used to implement GTD is to express the scattered field as a product of

$$\vec{E}^{s} = \Gamma\, A_d(s) e^{iks} \overline{\overline{D}} \cdot \vec{E}^{i}$$

where

Γ = Reflection coefficient,
$A_d(s)$ = Ray spreading factor,
e^{iks} = Phase variation relative to the specular point,
$\overline{\overline{D}}$ = Diffraction matrix which relates the incident to the scattered electric field at the diffraction point.

$$\overline{\overline{D}} = \begin{bmatrix} D_{\parallel} & 0 \\ 0 & D_{\perp} \end{bmatrix}$$

where

$D_{\parallel}, D_{\perp}$ = Scalar diffraction coefficients.

Shown in Reference 4, the D is based on exact solution of the canonical problem of diffraction such as the wedge diffraction coefficients:

$$D^{s,h} \sim \frac{(2/n)\sin(\pi/n)}{\sqrt{(8/\pi k)}\ \sin\beta_o}\left\{\left[\cos\left(\frac{\pi}{n}\right) - \cos\left(\frac{\phi-\phi_o}{n}\right)\right]^{-1} \mp \left[\cos\left(\frac{\pi}{n}\right) - \cos\left(\frac{\phi+\phi_o}{n}\right)\right]^{-1}\right\}$$

where

n	=	$(2\pi - \alpha)/\pi$ with α as the interior wedge angle.
β_o	=	The smaller angle between the direction of incidence and the tangent at the point of incidence.
ϕ_o, ϕ	=	The angles of incidence and scattering, respectively.
s, h	=	Soft and hard wedges; s and h correspond to plus and minus, respectively.

Keller's diffraction coefficients [4] for a straight wedge are shown in Figure 2.

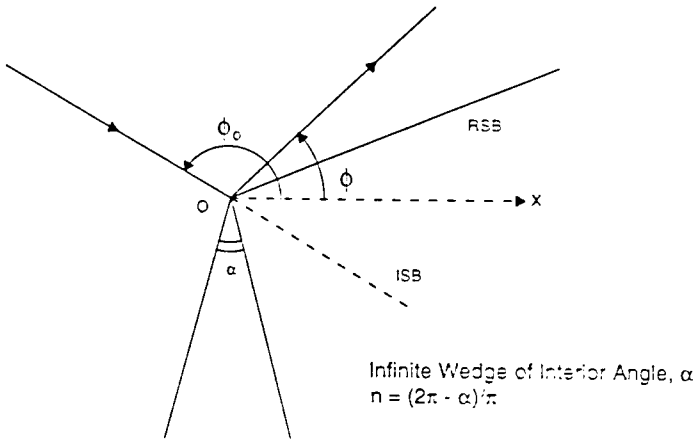

Figure 2. Diffraction of a Plane Wave by an Infinite Plane Wedge

Several limitations have been identified using GTD. These include: (1) the diffracted field becomes infinite at both incident and reflected shadow boundaries; (2) the diffraction coefficient becomes infinite at the edge, thereby breaking the edge condition; (3) the expression for diffraction coefficient has been acquired only by comparison with an exact solution of a canonical problem and does not follow as an integral part; (4) the higher–order terms in the expression for a diffracted wave cannot be determined; and (5) the solution becomes singular at a caustic [4].

C. Uniform Theories of Diffraction

Two different theories have been developed to handle the shadowing limitation observed in GTD. Reference 1 shows the development of the Uniform Asymptotic Theory (UAT) of diffraction. This was on the assumption that the field solution in an edge diffraction problem can be expanded in a particular asymptotic series implicating a Fresnel integral. The UAT solution is uniformly valid close to and away from the shadow boundaries [4].

The most popular method is UTD which was developed by Kouyoumjian and Pathak [4]. UTD can handle large–sized scattering objects in an efficient manner. The larger the object in terms of a wavelength, the better the solution. Complex objects can be systematically built up using the major local scattering centers based on diffraction coefficients [22]. The singularities in the diffraction coefficients are defeated by multiplying the diffraction coefficients by a Fresnel integral. At the shadow boundary, or the reflection boundary, the modifying Fresnel integral is zero while the diffraction coefficient is infinite. The product of the two stays finite [10].

Figure 3 shows the diffraction of an electromagnetic wave by a curved wedge [4].

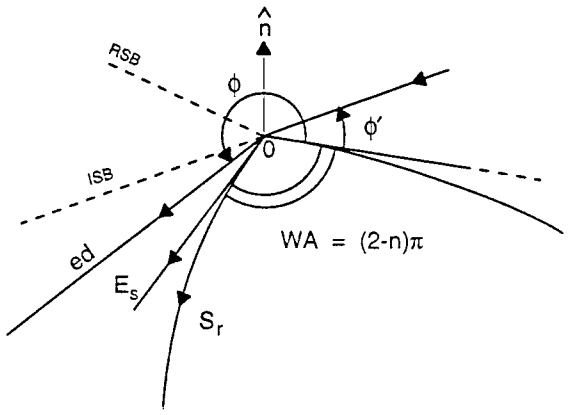

Figure 3. Diffraction by a Curved Wedge

Reference 4 gives the diffraction coefficients uniform at and around the shadow boundaries as:

$$D^{s,h}(\phi,\ \phi',\ \beta_o) = \frac{-\exp(i\pi/4)}{2n\sqrt{2\pi k}\ \sin\beta_o}$$
$$x\left\{\left\{F\left[kLa^+\ (\phi-\phi')\right]\cot\frac{\pi+(\phi-\phi')}{2n}\right.\right.$$
$$\left.+F\left[kLa^-\ (\phi-\phi')\right]\cot\frac{\pi+(\phi-\phi')}{2n}\right\}$$
$$\mp\left\{F\left[kLa^+\ (\phi+\phi')\right]\cot\frac{\pi+(\phi+\phi')}{2n}\right.$$
$$\left.\left.+F\left[kLa^-\ (\phi+\phi')\right]\cot\frac{\pi-(\phi-\phi')}{2n}\right\}\right\}$$

where

$$F(x) = 2i\sqrt{x}\ \exp^{ix}\int_{\sqrt{x}}^{\infty}\exp^{-i\tau^2}d\tau$$

$$a^{\pm}(\beta) = 2\cos^2\frac{2n\pi N^{\pm}-(\beta)}{2}$$

where $N^{\pm}$ are the integers that most nearly satisfy these equations:

$2\pi nN^{+}-(\beta) = \pi$ with $\beta = \phi+\phi'$,
$2\pi nN^{-}-(\beta) = \pi$ with $\beta = \phi-\phi'$.

L is a distance parameter defined as

$L = S^2\sin\beta_o$ for plane wave incidence,
$L = \frac{rr'}{r+r'}$ for cylindrical wave incidence,
$L = \frac{ss'}{s+s'}\sin^2\beta_o$ for conical and spherical wave incidence,
r' = radius of curvature of the cylindrical wave normally incident on the edge,
r = perpendicular distance of the field point from the edge,
S = distance along the ray from the edge to the observation point,
$N^{\pm}$ = functions of β and n,
β_o = the smaller angle between the direction of the incidence,

and the tangent is drawn at the point of incidence on the edge [4].

F(x) is a modified Fresnel integral which is shown approximated as [4]:

$$F(x) \cong \left[\sqrt{\pi x}-2x\ \exp(i\pi/4)-\frac{2}{3}\ x^2\ \exp(-i\pi/4)\right]\exp\left[i\left(\frac{\pi}{4}+x\right)\right] \quad \text{for } x<1$$

$$F(x) \cong \left(1+\frac{i}{2x}-\frac{3}{4}\frac{1}{x^2}-i\frac{15}{8}\frac{1}{x^2}+\frac{75}{16}\frac{1}{x^4}\right) \quad \text{for } x>1.$$

When the source is near the edge, the diffraction coefficient needs a correction considering the variation of incident field intensity along the edge of the wedge. This is known as the uniform slope diffraction correction. Reference 4 defines the uniform slope diffraction coefficient as:

$$\frac{\partial D_{s,h}(\phi,\ \phi';\ \beta_o)}{\partial \phi'} = -\frac{e^{-\pi/4}}{4n^2\sqrt{2\pi k}\ \sin\beta_O} x\left\{\left\{\csc^2\left[\pi + \frac{(\phi-\phi')}{2n}\right] F_s\left[kLa^+(\phi-\phi')\right] - \csc^2\left[\frac{\pi-(\phi-\phi')}{2n}\right] F_s\left[kLa^-(\phi-\phi')\right]\right\} \pm \left\{\csc^2\left[\frac{\pi+(\phi+\phi')}{2n}\right] F_s\left[kLa^+(\phi+\phi')\right] - \csc^2\left[\frac{(\pi-\phi+\phi')}{2n}\right] F_s\left[kLa^-(\phi+\phi')\right]\right\}\right\}$$

where

$$F_S(x) = 2ix + 4x^{3/2}e^{ix}\int_{\sqrt{x}}^{\infty} e^{-i\tau 2}\, d\tau$$

or

$$F_S(x) = 2ix[1 - F(x)].$$

At a shadow boundary, the following limit is used:

$$\csc^2\left(\frac{\pi \pm \beta}{2n}\right) F_S\left[kLa^{\pm}(\beta)\right] = 4ikLn^2\left(1 - \varepsilon\sqrt{\frac{\pi kL}{2}}\ e^{i\pi/4}\right)$$

where

$$\beta = 2\pi n N^{\pm}_{\mp}(\pi - \varepsilon)$$

and ε is small.

The disadvantages of UTD hinge on the fact that it is assumed that the most important mechanisms are known. If some terms are left out, the accuracy of the total solution may diverge; accuracy also depends on knowing the diffraction coefficients. As more terms are added to the solution, the more time it takes to trace and shadow the rays [22]. UTD cannot handle caustics nor the treatment of cross polarization [4].

D. Method of Equivalent Currents

MEC is an analytical tool using fictitious currents to overcome the caustic difficulties. MEC has the ability to predict the scattered fields in the direction of a caustic, to calculate the diffracted fields from an edge of finite length and for observation angles away from the cone of diffracted rays, and to find the reflected fields from curved bodies of finite length [19].

The basic approach is to assume the existence of electric and magnetic currents at each point around the edge contour and sum them in the far field radiation integral [12]

$$\bar{E}_d = -ik\Psi_o \int \left[Z_o I_e \hat{s} \times \left(\hat{s} \times \hat{t} \right) + I_m \left(\hat{s} \times \hat{t} \right) \right] e^{-ik\hat{r}\cdot\hat{s}} \, dt$$

Ψ_o = Far field Green's function,
$\hat{t}$ = Unit vector aligned along the contour.

Millar, Ryan and Peters, Knott and Senior, and Michaeli have used equivalent currents in many of their studies. Equivalent currents proposed by Ryan and Peters are

$$I_e = i2(X - Y) \left(\hat{t} \cdot \bar{E}_i \right) / kZ_o$$

$$I_m = i2(X + Y) \left(\hat{t} \cdot \bar{H}_i \right) / kZ_o \, .$$

where

$$X = \frac{(1/n) \sin(\pi/n)}{\cos(\pi/n) - \cos\left[(\Psi_s - \Psi_i)/n \right]}$$

$$Y = \frac{(1/n) \sin(\pi/n)}{\cos(\pi/n) - \cos\left[(\Psi_s + \Psi_i)/n \right]}$$

n = Exterior wedge angle normalized with respect to π.
Ψ_i, Ψ_s = Angles of the transverse components of the incident and diffracted directions with respect to one of the surfaces meeting at the edge.

When these currents are used in the far field radiation integral, all scattered fields are obtained. To extend MEC to general bistatic cases, Knott and Senior interpreted the product:

$$\sin^2 \beta = \sin \beta_i \sin \beta_s$$

where i and s denote the angle subtended by the incident and scattering directions. Reference 12 denotes when the equivalent currents are placed in the far field radiation integral, the result is a contour integral:

$$\bar{E}_d = -2E_o\Psi_o \int_C \frac{e^{ik\hat{r}\cdot(\hat{i}-\hat{s})}}{\sin \beta_i \sin \beta_s}$$

$$x \left[\left(\hat{t} \cdot \hat{e}_i \right) (X - Y) \, \hat{s} \times \left(\hat{s} \times \hat{t} \right) + \left(\hat{t} \cdot \hat{h}_i \right) (X + Y) \hat{s} \times \hat{t} \right] dt$$

$\hat{e}_i$ = Unit vector aligned along incident electric field.
$\hat{h}_i$ = Unit vector aligned along incident magnetic field.
C = Illuminated portions of the edge.

Michaeli devised a completely different set of diffraction coefficients considering the far field contribution due to two narrow surface strips (one on each face of a wedge) meeting at an edge element and integrated the induced currents along the strips.

A disadvantage of MEC is the complexity of the diffraction coefficients. This may prohibit the implementation of the method for complex bodies which is composed of hundreds of facets [4].

E. Physical Optics

PO overcomes the infinities of flat and singly curved surfaces prominent in GO by approximating the induced surface fields and integrating them to obtain the scattered field [12]. PO is a high–frequency technique where the target is replaced by induced surface currents that serve as the source of scattered fields. In obtaining the currents, it is assumed that: (1) the radii of curvature of the surface are large compared to wavelength, and (2) currents exist only in the area that is directly illuminated by the incident wave and currents on the illuminated surface have the same characteristics as those on the infinite plane tangent to the surface at the point of incidence [4]. PO relies on the estimates of the surface fields from GO [10].

Reference 14 noted twelve different interpretations of PO. These depend on the choice of current distribution on the target surface and other characteristics. Reference 4 gives three possible choices of the currents on the target surface as:

$$\text{E}-\text{H–Formulation:}\quad J_s = \hat{n}\times\left(\mathbf{H}^1+\mathbf{H}^s\right);\quad M = \left(\mathbf{E}^i+\mathbf{E}^s\right)\times\hat{n}$$

$$\text{H–Formulation:}\quad J_s = 2\left(\hat{n}\times\mathbf{H}^i\right);\quad M = 0$$

$$\text{E–Formulation:}\quad J_s = 0;\quad M = 2\left(\mathbf{E}^s\times\hat{n}\right)$$

where $\mathbf{E}^i$, $\mathbf{H}^i$ and $\mathbf{E}^s$, $\mathbf{H}^s$ are the incident and scattered fields at the target surface and are related by boundary conditions.

In general, PO current is imbedded as an unknown in an integral equation whose solution provides the required current for field calculations. Reference 4 explained that ignoring the effects of any surface current in the direction of observation, the Stratton–Chu equations are modified to give the scattered fields:

$$\mathbf{E}^s = +i\frac{e^{-k_o r}}{r}\int_s \hat{s}\times\left(\mathbf{M}+\eta_o\hat{s}\times\mathbf{J}_s\right)\exp\left[ik_o r'\cdot\left(\hat{i}-\hat{s}\right)\right]ds'$$

$$\mathbf{H}^s = -i\frac{e^{-k_o r}}{r}\int_s \hat{s}\times\left(\mathbf{J}_s+\frac{1}{\eta_o}\hat{s}\times\mathbf{M}\right)\exp\left[-ik_o r'\cdot\left(\hat{i}-\hat{s}\right)\right]ds'.$$

where

$\hat{i},\hat{s}$ = Unit vectors in the directions of incidence and observation.
S = Illuminated portion of target surface.

All other parameters are shown in Figure 4 [4].

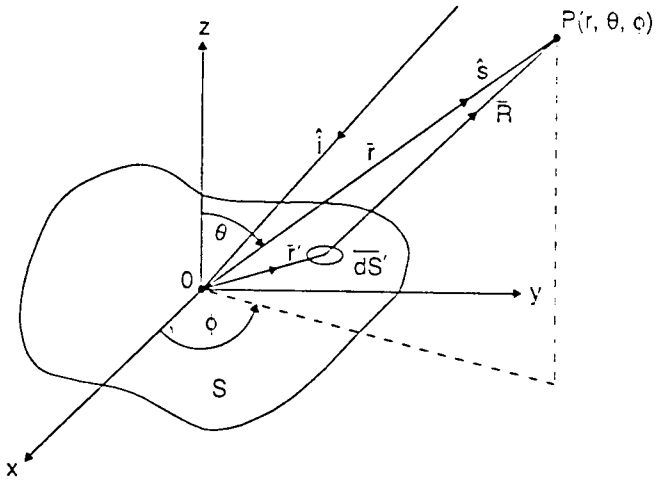

Figure 4. Electromagnetic Scattering from a Surface

The two equations above may be considered the generalized PO formulation and are used to obtain the scattered field with a knowledge of the currents $\mathbf{J_s}$ and $\mathbf{M}$ obtained either by solving appropriate integral equations or by suitable approximations [4].

The accuracy of PO can be improved by improving the assumed current distributions. In PO, the contributions from edges are ignored. Disadvantages include: (1) cannot predict currents due to a discontinuity on a body; (2) cannot handle depolarization for a monostatic single scatterer; (3) cannot predict diffraction effects (shadow region fields); and (4) is considered inaccurate for wide–angle lobe predictions [4].

F. Physical Theory of Diffraction

A more accurate representation of the scattered fields than PO was developed by Ufimtsev, known as PTD. PTD was developed for treating edges. Ufimtsev represented the scattered field as the sum of the PO contribution and an edge contribution, using the exact solution of the two–dimensional wedge problem [12].

Using Sommerfeld's solution of the wedge problem, Ufimtsev represented the incident field plus the scattered fields as:

$$E_z = E_{oz}\left[u(r,\ \Psi_s - \Psi_i) - u(r,\ \Psi_s + \Psi_i)\right]$$

$$H_z = H_{oz}\left[u(r,\ \Psi_s - \Psi_i) + u(r,\ \Psi_s + \Psi_i)\right]$$

where

$$u(r,\ \Psi) = \frac{1}{2\alpha}\int_C \frac{e^{-ikr\cos\beta}}{1 - \exp[i\pi(\beta + \Psi)/\alpha]}\, d\beta$$

where r is the distance from the edge to the point of observation, Ψ_s is the angular coordinate of that point above one face of the wedge, Ψ_i is the direction of arrival of the incident wave, α is the external wedge angle, and C is the Sommerfeld contour in the complex plane [12].

Depending on the direction of arrival of the incident wave, there are three possible PO contributions to subtract from the exact solution. One occurs if the upper face is illuminated, but not the lower face; another occurs if the lower face is illuminated, but not the upper; and the third occurs if both faces are illuminated [12]. Results will be given in different forms for the three different contributions. Ufimtsev's results are summarized below:

$$E_z^s = E_{oz}\, f\, \frac{e^{i(kr+\pi/4)}}{\sqrt{2\pi kr}}$$

$$H_z^s = H_{oz}\, g\, \frac{e^{i(kr+\pi/4)}}{\sqrt{2\pi kr}}$$

where the diffraction coefficients are

$$f = \begin{cases} (X - Y) - (X_1 - Y_1) & 0 \le \Psi_i \le \alpha - \pi \\ (X - Y) - (X_1 - Y_1) - (X_2 - Y_2) & \alpha - \pi \le \Psi_i \le \pi \\ (X - Y) - (X_2 - Y_2) & \pi \le \Psi_i \le \alpha \end{cases}$$

$$g = \begin{cases} (X + Y) - (X_1 + Y_1) & 0 \le \Psi_i \le \alpha - \pi \\ (X + Y) - (X_1 + Y_1) - (X_2 + Y_2) & \alpha - \pi \le \Psi_i \le \pi \\ (X + Y) - (X_2 + Y_2) & \pi \le \Psi_i \le \alpha . \end{cases}$$

Reference 12 describes the unsubscripted coefficients as Keller coefficients shown on page 13 of this report. The subscripted coefficients are due to the uniform PO contributions.

$$X_1 = -\frac{1}{2} \tan\left[(\Psi_s - \Psi_i)/2\right]$$

$$Y_1 = -\frac{1}{2} \tan\left[(\Psi_s + \Psi_i)/2\right]$$

$$X_2 = \frac{1}{2} \tan\left[(\Psi_s - \Psi_i)/2\right]$$

$$Y_2 = -\frac{1}{2} \tan\left[\alpha - (\Psi_s + \Psi_i)/2\right]$$

A disadvantage in using PTD is that it yields only the contributions due to edges. Some other method, such as PO, must be used to obtain the surface contributions [12].

IV. CURRENT MODELING APPLICATIONS

Distinct computer codes exist today for high–frequency RCS prediction. A major issue for code developers has been in the implementation of electromagnetic theory for practical applications [13]. The target is essentially divided into two parts: how the incident and scattered fields are related at a particular point on the target, and the interaction and combination of the scattered–field contributions from different points of the target [15].

Code development began in the early 1970's. One such code was MISCAT, developed by Northrop Corporation [18]. High–frequency computer codes have been ameliorated over the past several years. The most prevailing codes today include: XPATCH, RCS – Basic Scattering Code (RCS–BSC), Simulated Radar Image (SRIM), and MAX–TRACK.

A. XPATCH

XPATCH is a general purpose RCS prediction code used to calculate the polarimetric radar return from different targets. The code was developed by DEMACO, Inc. under the joint tri–Service sponsorship of Wright Laboratory at Wright–Patterson AFB, Ohio, Phillips Laboratory at Kirtland AFB, New Mexico, the Army Research Laboratory at Ft. Belvoir, Virginia, and the Naval Air Warfare Center at Pt. Mugu, California [2]. The first version was written in 1988; however, it wasn't until late 1991, after further development, that it was used in RCS prediction [13].

XPATCH consists of three parts: electromagnetics which includes XPATCH1, XPATCH2, XPATCH3, and XPATCH4; CAD and visualization tools; and a graphical user interface [13]. All codes within XPATCH may be used as independent units. ACAD is the preferred CAD system to use for developing input target files; however, other CAD systems may be used with XPATCH. There is a translator entitled "FRED" which will convert from solid geometry to surface geometry (facets) or the reverse.

XPATCH1 uses triangular facet files for input target geometry. While this format is common for air targets, many existing CAD models for ground vehicles were built using BRL–CAD. BRL–CAD uses combinatorial solid geometry where different geometric primitives (boxes, cones, ellipsoids, etc.) are combined using Boolean operations such as union, intersection, and subtraction. XPATCH2 uses the solid geometry models [13].

SAR images were being developed using the traditional FFT method. For each SAR image, the scattered field from the target was typically calculated for 256 incident angles and 256 frequencies before the 2D Fast Fourier Transformation (FFT) was taken. Computer time was extensive. A direct shooting and bouncing ray technique was implemented in XPATCH3, which uses triangular facet files for target geometry, and XPATCH4, which uses the solid geometry target files as input [13].

XPATCH is currently based on the Shooting and Bouncing Ray (SBR) technique. Reference 3 has recognized the advantage of SBR and have pursued establishing its validity. In SBR, a dense grid of rays is emitted from the radar direction toward the target. These rays are traced according to the GO theory as they bounce from one part of the geometry to another and then exist. The tracing includes the effects of polarization, ray divergence factor, and layered material reflection. At the point where a ray exits the target, a frequency domain or time domain PO integration is done to calculate the scattered far field from the target. All single and multiple bounce contributions are accounted for by the GO or PO theory [13]. This ray bouncing technique is completely adequate for an aperture opening large compared to the wavelength; however, as the opening is decreased, additional features of the actual field must be accounted for in Reference 16.

Reference 16 indicates the bouncing technique that is carried out in three parts:

1. Given the geometry of the cavity and the incident field, the ray paths in the cavity must be found by ray tracking.

2. Determine the field amplitude of the exit rays on the aperture based on geometrical optics. The ray tube divergence factors and the reflection coefficients must be calculated.

3. Determine the backscattered field and the RCS using Kirchhoff's approximation (physical optics).

Following is a general description of these three steps.

Parallel rays are launched from the incident direction. Each ray is represented by a line in space with a reference point (x_o, y_o, z_o) and a direction vector (s_x, s_y, s_z). Any point (x_1, y_1, z_1) along this line is described by

$$(x_1, y_1, z_1) = (x_o, y_o, z_o) + (s_x, s_y, s_z)t$$

where t is time. If the phase of the field at (x_1, y_1, z_1) lags point (x_o, y_o, z_o), t is a positive quantity. The direction vector of the incident rays is given by

$$s_x = -\sin\theta^i \cos\phi^i$$

$$s_y = -\sin\theta^i \cos\phi^i$$

$$s_z = -\cos\theta^i.$$

The reference point (x_o, y_o, z_o) on the incident plane Σ^i can be related to the point $(x_a, y_a, 0)$ on the aperture Σ_A by

$$x_o = \left(s_y^2 + s_z^2\right)x_a - s_x s_y y_a + s_x t_o$$

$$y_o = \left(s_x^2 + s_z^2\right)y_a - s_x s_y x_a + s_y t_o$$

$$z_o = -s_x s_z x_a - s_y s_z y_a + s_z t_o .$$

The t_o above determines how far Σ^i is from the aperture plane and can be chosen arbitrarily [10].

Once the incident rays have been defined, the impact point of each ray on the inner wall of the cavity can be determined. This is achieved by the equation describing the cavity $z = (f(s, y))$ and any point. For example, if the cavity is a circular cylinder with radius a, the intersection is found by substituting into the equation for any point along the line

$$t = \left(-B + \sqrt{B^2 - 4AC}\right)/2A$$

where

$$A = s_x^2 + s_y^2$$
$$B = 2\left(s_x x_o + s_y y_o\right)$$
$$C = x_o^2 + y_o^2 - a^2 .$$

The reflected ray must satisfy Snell's law, such as it must lie in the plane of incidence and the angle of reflection must equal the angle of incidence. From Figure 5, Reference 16 defines a unit vector by

$$\hat{m} = \left(\hat{10} \times \hat{n}\right)/\sin\,\theta_c^i$$

$\hat{m}$ = Perpendicular to the plane of incidence.
$\hat{10}$ = Unit vector pointing from point 1 to point .0.

The departure of the ray from the cavity is easily detected when the ray intersects the aperture Σ_A. For every ray launched, a set of impact points inside the cavity and the direction of the exiting ray are obtained [16].

Once the ray paths inside the cavity are found, the field amplitude can be established. For each ray launched, a set of impact points is found inside the cavity. The aperture field associated with the exit ray can be determined. Using GO, the electric field obeys the following relationship:

$$\vec{E} = \left(x_{\bar{i}+1},\ y_{\bar{i}+1},\ z_{\bar{i}+1}\right) = (DF)_i \cdot \left(\overline{\overline{\Gamma}}\right)_i \cdot \vec{E}\left(x_{\bar{i}},\ y_{\bar{i}},\ z_{\bar{i}}\right) \cdot e^{-j(\text{phase})}$$

where

$$\text{phase} = k_o\left[\left(x_{i+1} - x_i\right)^2 + \left(y_{i+1} - y_i\right)^2 + \left(z_{i+1} - z_i\right)^2\right]^{1/2}.$$

$\vec{E}\left(x_{\bar{i}},\ y_{\bar{i}},\ z_{\bar{i}}\right)$ = Incident Field at (x_i, y_i, z_i).

$\left(\overline{\overline{\Gamma}}\right)_i$ = Planar reflection coefficient matrix at the i^{th} reflection point where the original curved interface (Fig. 5) is replaced by its tangent plane at the reflection point.

$(DF)_i$ = Divergence factor which governs the spreading of the differential ray tube from just after the i^{th} reflection to just before the $(i + 1)^{th}$ reflection.

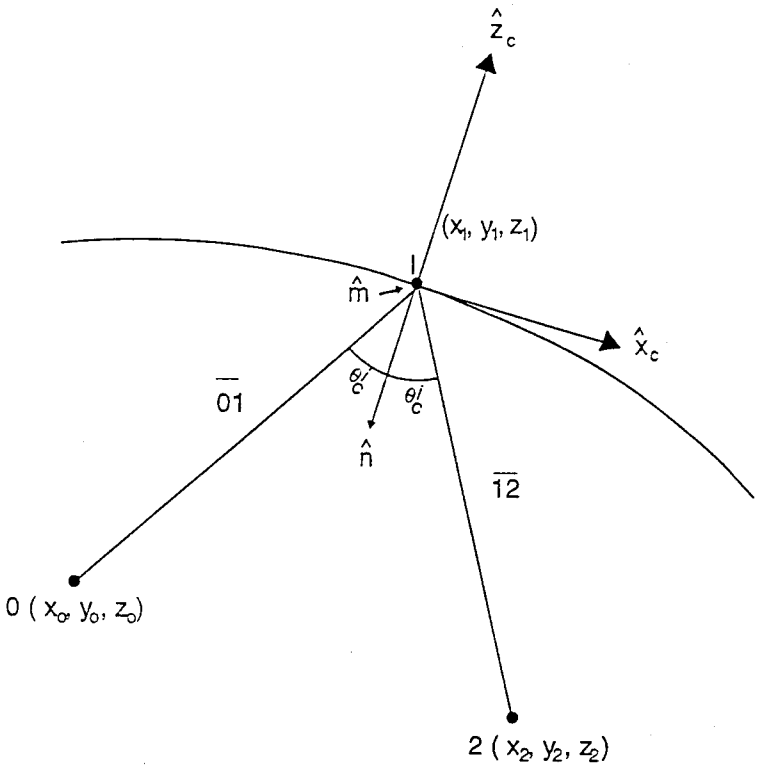

Figure 5. Local Coordinate System of a First Impact Point

The remaining task for amplitude tracking is to determine the planar reflection coefficients and the incident field.

In determining the backscattered field and the RCS, PO is used. The outgoing field is replaced by an equivalent magnetic current sheet

$$\vec{K}_s = \begin{cases} 2\vec{E}\,(x_N,\ y_N,\ 0) \times \hat{z}; & \text{over } \Sigma_A \\ 0 & \text{outside } \Sigma_A \end{cases}$$

$\vec{K}_s$ = Radiates in the backscattering direction and gives rise to the RCS.

The backscattered field is calculated from

$$\vec{E}^{bs} = \frac{e^{-jk_o r}}{r}\left[\hat{\theta}^i A_\theta + \hat{\phi}^i A_\phi\right]$$

$$\begin{bmatrix} A_\theta \\ A_\phi \end{bmatrix} = \frac{jk_o}{2\pi}\int\int_{\Sigma_A} dxdy\ e^{jk_o(ux+vy)} \cdot \begin{bmatrix} E_x \cos\phi^i + E_y \sin\phi^i \\ \left(-E_x \sin\phi^i + E_y \cos\phi^i\right)\cos\theta^i \end{bmatrix}$$

$u = \sin\theta^i \cos\phi^i$
$v = \sin\theta^i \sin\phi^i.$

E_x and E_y are the x and y components of the outgoing field on the aperture Σ_A. The PO integral defined above is evaluated by summing the backscattering contributions due to each ray tube. The RCS is shown in Table 1 [16].

Table 1. Radar Cross Section Definition

	$\perp$ Polarization (l=1, $\bar{\mathrm{l}}$=0)	$\parallel$ Polarization (l=0, $\bar{\mathrm{l}}$=1)
Co–pol	$RCS_{\phi\phi} = 4\pi \lvert A_\phi \rvert^2$	$RCS_{\theta\theta} = 4\pi \lvert A_\theta \rvert^2$
Cross–pol	$RCS_{\theta\phi} = 4\pi \lvert A_\theta \rvert^2$	$RCS_{\phi\theta} = 4\pi \lvert A_\phi \rvert^2$
Phase	$\angle A_\phi$, $\angle A_\theta$	$\angle A_\theta$, $\angle A_\varphi$

l = Amplitude of perpendicular (vertical) polarization
$\bar{\mathrm{l}}$ = Amplitude of parallel (horizontal) polarization.

The validity of XPATCH results are susceptible to: (1) user selected input parameters, (2) measurement error of data used in the validation process, (3) facetization levels, and (4) the electrical size (wavelength versus object size). All of these factors are extremely important [9].

XPATCH provides realistic RCS, range profiles, and 2–D SAR imagery calculations for complex targets; however, model deficiencies exist. These include poor or missing detail, inaccurate surface curvature, and improper modeling of small features and materials. The computer code does not currently perform some of the higher order scattering effects such as traveling waves, surface waves, resonant effects, and creeping waves [2]. Upgrading of XPATCH is continuous. Research is ongoing to quantify the level of fidelity required for different frequency ranges and applications.

B. Radar Cross Section – Basic Scattering Code

ElectroScience Laboratory of the Ohio State University has developed the user–oriented Radar Cross Section – Basic Scattering Code (RCS–BSC) which provides far zone scattering from complex structures. The first version was published in 1979, and a second version followed during 1990, [24].

RCS–BSC does not interface with large CAD data descriptions of target geometry. All target modeling is simulated within the program through the use of basic shapes. The basic shapes include multiple–sided flat plates, multiple–section cone frustums, and finite–composite section ellipsoids [22]. A multiple sided flat plate or a box type structure that is composed of a number of multiple sided plates attached together at corners can be analyzed with all its dominant terms. All finite plates and curved surfaces have to be perfectly conducting. The infinite ground plane can be dielectric [17].

Once all of the required target geometry is input into the code, RCS–BSC analyzes the data and puts it into the correct form so that the electric and magnetic fields as well as coupling information can be calculated. A complete set of incident and scattering polarizations is analyzed [17]. The analysis is made from uniform asymptotic techniques formulated from GTD. The principal result is found by summing the diffracted field from every corner or edge visible to the incident and observation directions [17] corner diffraction coefficients are based on Michaeli's equivalent currents [8]. The simulation code contains double diffracted fields from the corner to edge, edge to corner, and corner to corner. It also contains edge wave effects and multiple plate to plate interactions [17]. Overall, the code encompasses finding closed form solutions for PO and currents and asymptotically matching them to UTD solutions and formats [17].

The code calculates the incident field as

$$\vec{E}^{i} = \hat{e}^{i} E^{i}_{o} e^{jk\vec{r}'\cdot\hat{r}^{i}}$$

$$\hat{e}^{i} = \hat{\theta}^{i}, \hat{\phi}^{i}.$$

Both incident polarizations are calculated at the same time. The incident magnitude, E^{i}_{o}, is assumed to be one volt/meter.

Reference 8 provides detailed derivations of all theoretical techniques used in RCS–BSC. These include: (1) the corner diffraction coefficients; (2) the relation that exists between electromagnetic surface currents on a wedge and equivalent currents in free space that would radiate at high frequencies in the same way as the wedge surface currents; (3) the electromagnetic fields that result when a plane wave impinges on a wedge; (4) Michaeli's fringe and PO equivalent currents used; and (5) the corner diffraction coefficients that result from the use of Michaeli's equivalent currents to determine the corner diffraction coefficients.

RCS–BSC was designed to complement other techniques. It is a fast and cost effective means of optimizing parameters and anticipating problems at the early design stages of a system. The code can handle only a limited number of scatterers and has tight constraints on required surface types; therefore, it is not considered the best code for complex targets.

C. Simulated Radar Image

Another fully polarimetric computer code available today for high–frequency RCS prediction is the SRIM code. The code has been under development for several years with particular emphasis being placed on the simulation of polarimetric sensor systems. Reference 7 has outlined the simulation process shown in Figure 6.

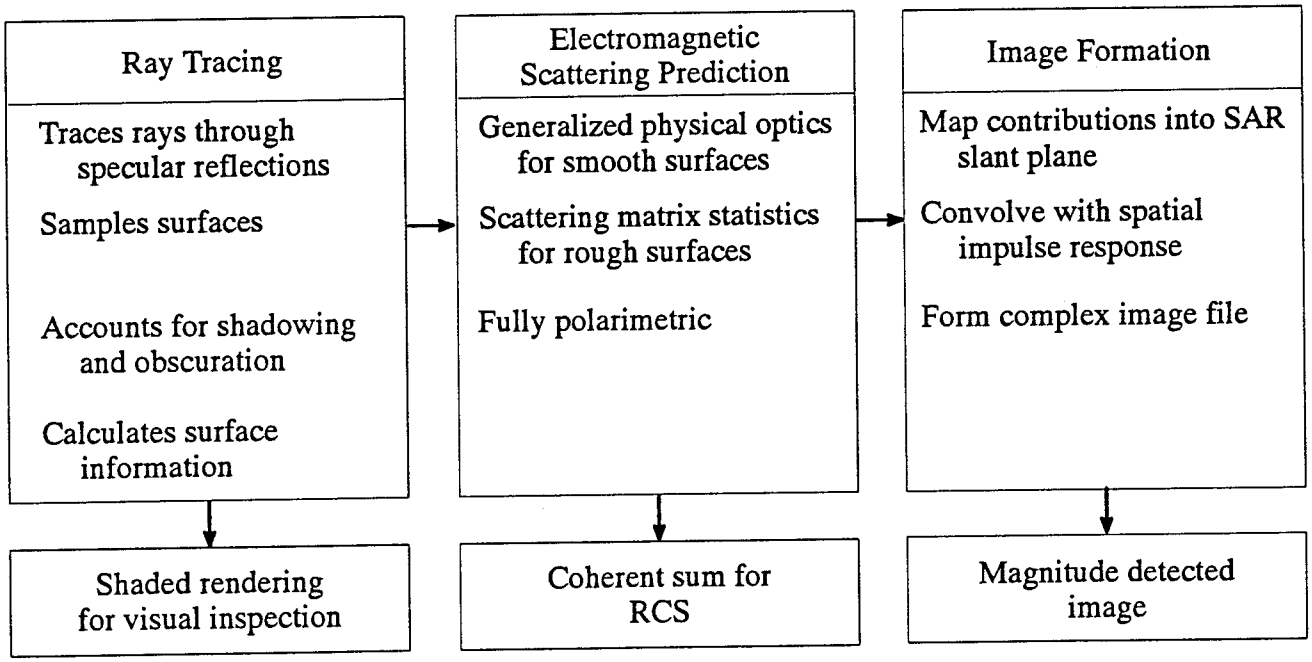

Figure 6. SRIM Processing

The first step is the construction and sampling of a three–dimensional model of the target and scene geometry. The target is modeled using constructive solid geometry and boundary representation. The ground region is specified in terms of the contour of its underlying smooth surface. Ray tracing samples target surfaces and generates surface information for the scattering calculation. Each surface of the geometry model is assigned a set of attributes which determines the model used to compute the scattered field. These attributes include whether the surface is smooth or rough and whether it is perfectly or finitely conducting [7].

Scattering from smooth surfaces is computed from a generalization of the PO approximation. Scattering from rough surfaces is computed by drawing realizations from the first– and second–order statistical moments of polarization scattering matrix. These moments are obtained from experimental data or analytical models [7].

RCS is calculated by coherent summation of the scattered fields. Three RCS values are computed: isolated target RCS, interacting target RCS, and ground terrain RCS per unit area [26]. The backscattered field contribution is mapped to coordinates in the image plane and convolved with the system impulse response to form the complex polarimetric image [7].

The following mathematical formulation [7] describes the SAR simulation as the predominant point of view. Letting α and β denote the receive and transmit polarizations of the radar and u(t) the transmitted waveform, the radar return signal is modeled as

$$v_{\alpha\beta}(t) = K \int_S \gamma_{\alpha\beta}(\bar{r}')\, u(t - 2R/c)\, ds'$$

where

R = Radar Range

S = Illuminated Surface

$\gamma_{\alpha\beta}$ = Scalar Reflectivity Density.

For smooth surfaces, this will lead to an explicit formula for the reflectivity density.

Defining a dyadic reflectivity where

$$\gamma_{\alpha\beta} = \hat{h}_\alpha \cdot \bar{\bar{\gamma}} \cdot \hat{h}_\beta$$

$\hat{h}_\alpha$ = Magnetic field polarization vector of receive antenna

$\hat{h}_\beta$ = Magnetic field polarization vector of transmit antenna

you obtain:

$$\bar{\bar{\gamma}}(\bar{r}') = -0.5\, \hat{r} \times \left[\hat{n} \times \left(\bar{\bar{I}} + \bar{\bar{R}}_H\right) + \hat{r} \times \hat{n} \times \left(\bar{\bar{I}} + \bar{\bar{R}}_E\right) \times \hat{r}\right]$$

$\hat{n}$ = Surface normal,

$\hat{r}$ = Radar aspect,

$\bar{\bar{I}}$ = Identity dyadic,

$\bar{\bar{R}}_H$, $\bar{\bar{R}}_E$ = Fresnel reflection dyadics.

SRIM computes the contribution of the n^{th} reflection point to the p^{th} image pixel as

$$\overline{\overline{g}}(\bar{r}_p, \bar{r}_n) = K \int_{\delta S_n} a(\bar{r}_p - \bar{r}') \, \overline{\overline{\gamma}}(\bar{r}') \, e^{i2\pi \bar{f}_o \cdot \bar{r}'} \, ds'$$

$$\sim a(\bar{r}_p - \bar{r}_n) \, e^{i\phi_n} \, \overline{\overline{\Gamma}}_n$$

$a(\bar{r})$ = Spatial impulse response of the radar,
δS_n = Surface patch illuminated at sample point,
ϕ_n = $2\pi \bar{f}_o \cdot \bar{r}'$,
$\bar{f}_o$ = $(2/\lambda_o)\,\hat{r}$.

For a smooth surface, the reflectivity density γ is a continuous function over the target surface. The sampled reflectivity Γ is determined by integrating over a surface patch the product of γ with a position–dependent phase function. An exact analytical evaluation of the integral is used for planar surfaces, and a stationary phase evaluation is used for curved surfaces [26]. For smooth surfaces:

$$\overline{\overline{\Gamma}}_n = K \int_{\delta S_n} \overline{\overline{\gamma}}(\bar{r}') \, e^{i2\pi \bar{f}_o \cdot (\bar{r}' - \bar{r}'_n)} \, ds' .$$

For rough surfaces, it is not possible to define a continuous reflectivity density. It is assumed that optically rough surfaces result in noncoherent diffuse scattering. Using the central limit theorem, the components of the scattered field are modeled as complex circular Gaussian random variables.

$$\overline{\overline{\Gamma}} = \sqrt{4\pi} \, \overline{\overline{F}}_n$$

$\overline{\overline{F}}_n$ = Magnetic field scattering matrix.

SRIM is a more antiquated code. It contains multiple interactions and calculates reflection; however, no diffraction calculations are included.

D. MAX–TRACK

Under various Government contracts, Georgia Tech Research Institute (GTRI) has developed MAX–TRACK, which is essentially two programs interacting with one another. A geometric description of the target is entered using MAX; then the model description from MAX is used as input into the radar modeling program called TRACK [6]. TRACK uses PO, GO, and MEC to predict the returns from the discrete reflective targets [23]. The output from TRACK may be used for post–processing into SAR or ISAR imagery, range only output, azimuth/elevation profile, raster scan image, doppler spectra, or Doppler Beam Sharpening (DBS) image [6]. A general description of each program follows.

MAX was developed to create and modify models which TRACK could use to predict targets. It stores all the information needed to accurately describe target geometry and material properties. These models are a collection of simple geometric shapes which describe the surface geometry of a three–dimensional object. Elements currently supported include generalized elliptical cone frusta, triangular and quadrilateral flat plates, generalized ellipsoids, dihedrals and trihedrals, tophats, hermite patches, and generalized elliptical toroids. Figure 7 illustrates these simple element shapes. These elements are organized into a hierarchical structure of groups and nodes [6].

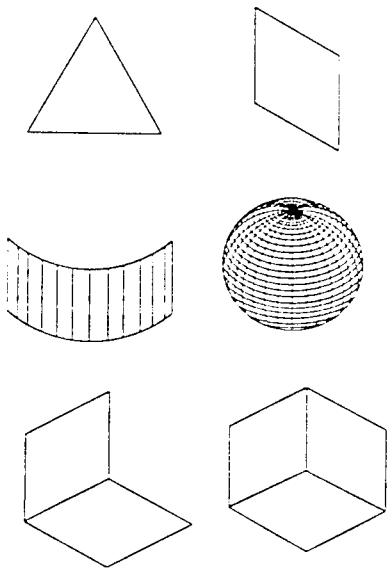

Figure 7. Element Shapes Used by MAX

TRACK predicts the RCS. After calculating the return from the individual scattering centers on the target, TRACK can either coherently sum the individual returns or retain the complex polarization scattering matrix from each scatterer for image post–processing [6]. The scattered returns from each element of the target model, except multiple scatter elements, are calculated with the PO integral. Multiple bounce reflections which occur for multiple scatter elements are treated with a combination of GO and PO techniques. The scattered field from straight edges is calculated with MEC [5].

These formulations are modified by a diffuse scattering algorithm which accounts for the roughness of the individual scattering elements. From this, the diffuse scatter from dielectrics and conductors is calculated [5].

MAX–TRACK is predominantly used for simple target shapes; however, modifications are on–going for managing the more complex targets. Since the code uses beam tracing rather than ray tracing, its computer run time is much faster than some of the other codes.

V. FUTURE DIRECTION

Deriving a radar signature model through the use of a three–dimensional target drawing database has long been the dream of radar developers. This type of model would provide a cost effective alternative to real data collections and would allow us to exploit operational parameters. Through today's computational ability, the dream of an automated and systematic approach to theoretical RCS prediction is possible.

Future direction for high–frequency target modeling includes adding background in the models, development of a near–field version, and development of a hybrid code where different materials such as the wings on an airplane or blades on a helicopter can be incorporated. Reduction of computer run time continues to be crucial. Many of the existing codes take weeks to predict the RCS for one complex target. Accuracy is critical.

A great deal of effort has been placed in standardizing and validating the existing RCS simulation codes. An organization chartered as the Electromagnetic Code Consortium (EMCC) was formed by representatives of three U. S. DOD services and NASA in 1987 to integrate U. S. efforts on the development of electromagnetic codes, and to be a focal point for advancing the state–of–the–art in RCS code development and research [25]. The organization's efforts include participation from industry as well as university scientists and engineers.

Modern high–frequency codes are migrating toward the use of ray tracing as a means of computing the scattered field from complex objects. Using this technique, XPATCH is considered by the EMCC as the code to use today for high–frequency modeling [21]. Refinements, as well as additional capabilities, are being made continuously.

Extensive effort continues in the development of new codes as well as improving existing codes. These models must to be accurate, efficient, and user friendly [20].

REFERENCES

1. Ahluwalia, D. S., R. M. Lewis, and J. Boersma. 1968. "Uniform Asymptotic Theory of Diffraction by a Plane Screen. " SIAM J. Applied Math, 16 (July), pp. 783–807.

2. Andersh, D. J., S. W. Lee, F. L. Beckner, M. Gilkey, R. Schindel, M. Hazlett, and C. L. Yu. 1994."XPATCH: A High Frequency Electromagnetic Scattering Prediction Code Using Shooting and Bouncing Rays." Proc. Conf. on Applied Computational Electromagnetics (Monterey, California), 2 (Mar.), pp. 424–427.

3. Baldauf, J., S. W. Lee, L. Lin, S. K. Jeng, S. M. Scarborough, and C. L. Yu. 1991. "High Frequency Scattering from Trihedral Corner Reflectors and Other Benchmark Targets: SBR Versus Experiment." IEEE Transactions on Antennas and Propagation, 39 (Sep.), pp. 1345–1351.

4. Bhattacharyya, A. K., and D. L. Sengupta. 1991. Radar Cross Section Analysis and Control. (Norwood, MA: Artech House).

5. Davis, J. L., G. J. Bradley, R. B. Rakes, J. H. Andrews, M. T. Tuley, and P. A. Ryan. 1990. "TRACK 4.1 Radar Cross Section and Tracking Simulation User's Guide." NAVSEA 05T, Washington, DC, July.

6. Georgia Tech Research Institute, Signatures Technology Laboratory. 1994. "Radar Cross Section Modeling Software." May.

7. Herrick, D. F. 1988. "Computer Simulation of Polarimetric Radar and Laser Imagery." Proc. of the NATO Advanced Research Workshop on Direct and Inverse Methods in Radar Polarimetry (Bad Windsheim, Germany), Sep., Kluwer Academic Publishers, c 1992, pp. 1449–1453.

8. Jarem, J. M. 1989. "A Complete Derivation of Michaeli's Equivalent Currents and their Application to the Corner Diffraction Coefficients of the OSU RCS–BSC Computer Code." Final Report, University of Alabama in Huntsville, May.

9. Jernejcic, R. O., A. J. Terzuoli, Jr., and R. F. Schindel. 1994. "Evaluation of Radar Signature Predictions Using XPATCH." Proc. Conf. on Applied Computational Electromagnetics (Monterey, California), 1 (Mar.), pp. 343–345.

10. Knott, E. F., J. F. Shaeffer, and M. T. Tuley. 1985. Radar Cross Section (Norwood, MA: Artech House).

11. Knott, E. F. 1985. "A Progression of High–Frequency RCS Prediction Techniques." Proc. IEEE, 73 (Feb.), pp. 252–264.

12. Knott, E. F., J. F. Shaffer, and M. T. Tuley. 1993. Radar Cross Section, Second Edition. (Norwood, MA: Artech House).

13. Lee, S. W., D. J. Andersh, D. D. Reeves, S. K. Jeng, and H. Ling. 1993. "User Manual for XPATCH." DEMACO, Inc., Distributed by Electromagnetic Code Consortium, Sep.

14. Lee, S., J. Baldauf, H. Ling, and R. Chou. 1988. "Twelve Versions of Physical Optics: How Do They Compare?" IEEE AP–5 Symp. Dig., Syracuse, New York, pp. 408–411.

REFERENCES (Continued)

15. Lees, P. A., and M. R. Davies. 1990. "Computer Prediction of RCS for Military Targets." Proc. IEE, 137 (Aug.), pp. 229–236.

16. Ling, H., R. C. Chou, and S. W. Lee. 1989. "Shooting and Bouncing Rays: Calculating the RCS of an Arbitrarily Shaped Cavity." IEEE Transactions on Antennas and Propagation, 37 (Feb), pp. 194–205.

17. Marhefka, R. J. 1990. "Radar Cross Section – Basic Scattering Code, RCS–BSC (Version 2) User's Manual." Ohio State University, Technical Report 718295–15, Contract No. F33615–86–K–1023, United States Air Force Weight–Patterson AFB, Ohio, Feb.

18. McFarlin, M. S., and M. B. Murch. 1992. "RCS Prediction of Simple Target Measurement Data: Sphere, Cylinder, and Cone–Cylinder Test–Set." Simulation Technologies, Inc., Technical Report 131–109, Mar.

19. McNamara, D. A., C. W. I. Pistorius, and J. A. G. Malherbe. 1990. Introduction to the Uniform Geometrical Theory of Diffraction. (Norwood, MA: Artech House).

20. Miller, E. K. 1988. "A Selective Survey of Computational Electromagnetics." IEEE Transactions on Antennas and Propagation, 36 (Sep.), pp. 1281–1305.

21. Moore, T. G., E. C. Burt, and F. P. Hunsberger. 1994. "On the Use of Ray Tracing for Complex Targets." Proc. Conf. on Applied Computational Electromagnetics. (Monterey, California), 2 (Mar.), pp. 328–334.

22. Newman, E. H., and R. J. Marhefka. 1989. "Overview of MM and UTD Methods at the Ohio State University." Proc. IEEE, 77 (May), pp. 700–708.

23. Ryan, P. A., and K. R. Aberegg. 1992. "Millimeter Wave Feasibility Study." Summary Report, GTRI Project A–9163, Contract DAAA21–90D–0020–0013, Aug.

24. Tuley, M. T. 1991. "Radar Cross Section Model Evaluation." Georgia Institute of Technology, GTRI Project A–8638, Contract DAAH01–89–D–A003, U. S. Army Missile and Space Intelligence Center, Mar.

25. Volakis, J. L. 1992. "Benchmark Plate Radar Targets for the Validation of Computational Electromagnetics Programs." IEEE Antennas and Propagation Magazine, 34 (Dec.), pp. 52–56.

26. Walsh, M., and C. L. Arnold. 1991. "SRIM User Reference Manual." ERIM; WRDC, Dayton, Ohio.

27. Youssef, N. N. 1989. "Radar Cross Section of Complex Targets." Proc. IEEE, 77 (May), pp. 722–734.

INITIAL DISTRIBUTION LIST

		Copies
IIT Research Institute ATTN: GACIAC 10 W. 35th Street Chicago, IL 60616		1
AMSMI–RD		1
AMSMI–RD–AS,	Mr. Powell	1
	Mr. Pittman	1
AMSMI–RD–AS–MM,	Dr. Emmons	1
	Mr. Sedenquist	1
	Mrs. Monk	5
	Mr. Garner	1
	Mrs. Read	1
	Mr. Mullins	1
AMSMI–RD–CS–R		15
AMSMI–RD–CS–T		1
AMSMI–GC–IP,	Mr. Fred Bush	1
AMCPM–ITTS–QG,	Ms. Haack	1
	Mr. Wible	1
SFAE–MSL–HD,	LTC Wilbourn	1
SFAE–MSL–HD–E–M,	Mr. Beck	1